Acta Crystallographica Section D
Biological Crystallography
ISSN 0907-4449

Structure of aldolase from *Thermus thermophilus* HB8 showing the contribution of oligomeric state to thermostability

Neratur K. Lokanath,[a] Ikuya Shiromizu,[a]‡ Noriyasu Ohshima,[a] Yuichi Nodake,[a] Mitsuaki Sugahara,[a] Shigeyuki Yokoyama,[b] Seiki Kuramitsu,[b] Masashi Miyano[c] and Naoki Kunishima[a]*

[a]Highthroughput Factory, RIKEN Harima Institute at SPring-8, 1-1-1 Kouto, Mikazuki-cho, Sayo-gun, Hyogo 679-5148, Japan, [b]Structurome Research Group, RIKEN Harima Institute at SPring-8, 1-1-1 Kouto, Mikazuki-cho, Sayo-gun, Hyogo 679-5148, Japan, and [c]Structural Biophysics Laboratory, RIKEN Harima Institute at SPring-8, 1-1-1 Kouto, Mikazuki-cho, Sayo-gun, Hyogo 679-5148, Japan

‡ Present address: Bioscience Laboratory, Mochida Pharmaceutical Co. Ltd, 722 Jimba-aza-uenohara, Gotemba, Shizuoka 412-8524, Japan.

Correspondence e-mail: kunisima@spring8.or.jp

Received 12 May 2004
Accepted 13 August 2004

PDB References:
T. thermophilus aldolase, 1j2w, r1j2wsf; DRP complex, 1ub3, r1ub3sf.

2-Deoxyribose-5-phosphate aldolase catalyzes a reversible aldol condensation of two aldehydes *via* formation of a covalent Schiff-base intermediate at the active lysine residue. The crystal structure of 2-deoxyribose-5-phosphate aldolase from *Thermus thermophilus* HB8 has been determined with and without the substrate at atomic resolution. This enzyme, which has a unique homotetramer structure, has been compared with the previously reported crystal structures of two orthologues from *Escherichia coli* and *Aeropyrum pernix*. In contrast to the similar α/β-barrel fold of the monomers, substantial quaternary structural differences are observed between these three enzymes. Further comparison of the subunit–subunit interface areas of these aldolases showed a clear positive correlation between the interface area and the living temperature of the source organism. From these results, it is concluded that the oligomeric state of 2-deoxyribose-5-phosphate aldolase is important for the thermostability and not for the catalytic function.

1. Introduction

Aldolases have been extensively investigated in order to understand the mechanism of carbon–carbon bond formation in living organisms. The fidelity of the bond formation is very important as it determines the chirality and thus the biological activity of the compounds. 2-Deoxyribose-5-phosphate aldolase (DERA; EC 4.1.2.14) catalyzes the reversible aldol reaction between the donor aldehyde acetaldehyde and the acceptor substrate glyceraldehyde-3-phosphate to generate 2-deoxyribose-5-phosphate (DRP; Valentin-Hansen *et al.*, 1982). Over the past decade, protein engineering based on the crystal structures of aldolases has contributed significantly to the understanding of DERA enzyme catalysis (Heine *et al.*, 2001; Sakuraba *et al.*, 2003). The reaction mechanism of DERA involves the formation of a Schiff-base intermediate with an active-site lysine, which is characteristic of class I aldolases (Gefflaut *et al.*, 1995).

DERA is a unique enzyme as it catalyzes the aldol reaction between two aldehydes, while other aldolases require a ketone and an aldehyde as substrates. Its substrate specificity makes it a biocatalyst of considerable utility (Barbas *et al.*, 1990). For instance, its specificity has been exploited for the generation of catalytic antibodies to catalyze aldol reactions for the synthesis of epothilones, a new class of anti-cancer agents of considerable pharmaceutical interest (Machajewski & Wong, 2000). Furthermore, DERA is also important in the field of organic chemistry, because the novel catalytic synthesis of compounds in a manner that poses least hazard to the environment is in great demand by the pharmaceutical and chemical industries (Koeller & Wong, 2001). Enzyme-

catalyzed aldol condensation involving a Schiff-base intermediate is often carried out in aqueous solution at neutral pH and room temperature (Kajimoto *et al.*, 1991). Thus, DERA is capable of catalyzing the asymmetric syntheses of a wide variety of organic compounds (Gijsen *et al.*, 1996).

Here, we present the refined crystal structures of DERA from *Thermus thermophilus* HB8 (*Tt*DERA) and its complex with DRP. We show that *Tt*DERA is present as a tetramer in the crystal as well as in solution. *Tt*DERA shares 32.1 and 37.7% sequence identity with DERAs from *Escherichia coli* (*Ec*DERA; Heine *et al.*, 2001) and *Aeropyrum pernix* (*Ap*DERA; Sakuraba *et al.*, 2003), respectively. All these DERAs of known three-dimensional structure are oligomeric: *Ec*DERA is dimeric, while *Tt*DERA and *Ap*DERA are tetrameric. Although the reaction mechanism of DERA has been studied in detail, the biological role of its oligomeric state is not understood. In this paper, we present a comparison of these crystal structures and provide a rationale for the biological significance of the oligomeric state of DERA.

2. Materials and methods

2.1. Protein expression and purification

The gene coding for *Tt*DERA was amplified by the polymerase chain reaction (PCR) using *T. thermophilus* HB8 genomic DNA as the template. The PCR product was ligated with pT7blue (Novagen). The plasmid was digested with *Nde*I and *Bgl*II and the fragment was inserted into the expression vector pET-11a (Novagen) linearized with *Nde*I and *Bam*HI. *E. coli* BL21(DE3) cells were transformed with the recombinant plasmid and grown at 310 K in Luria–Bertani medium containing 50 µg ml^{-1} ampicillin for 20 h. The cells were harvested by centrifugation at 6500 rev min^{-1} for 5 min at 277 K and were subsequently suspended in 20 m*M* Tris–HCl pH 8.0 containing 0.5 *M* NaCl and 5 m*M* 2-mercaptoethanol. Cells were disrupted by sonication and heated at 343 K for 12 min. The cell debris and denatured proteins were removed by centrifugation (14 000 rev min^{-1}, 30 min). The supernatant solution was used as the crude extract for purification.

The crude extract was desalted with a HiPrep 26/10 desalting column (Amersham Biosciences) and applied onto a Super Q Toyopearl 650M (Tosoh) column equilibrated with 20 m*M* Tris–HCl pH 8.0 (buffer *A*). After elution with a linear gradient of 0–0.3 *M* NaCl, the fraction containing *Tt*DERA was desalted with a HiPrep 26/10 desalting column with buffer *A*. The sample was subjected to a Resource Q column (Amersham Biosciences) equilibrated with buffer *A*. After elution with a linear gradient of 0–0.4 *M* NaCl, the fraction containing *Tt*DERA was desalted with a HiPrep 26/10 desalting column with 10 m*M* sodium phosphate pH 7.0. The sample was then applied onto a Bio-Scale CHT-20-I column (Bio-Rad) equilibrated with 10 m*M* sodium phosphate pH 7.0. After elution with a linear gradient of 10–100 m*M* sodium phosphate, the fraction containing *Tt*DERA was subjected once more to a Resource Q column. The sample was concentrated by ultrafiltration (Vivaspin) and loaded onto a HiLoad 16/60 Superdex 75 prep-grade column (Amersham Biosciences) equilibrated with buffer *A* containing 0.2 *M* NaCl. The homogeneity and identity of the purified sample were assessed by SDS–PAGE (Laemmli, 1970) and N-terminal sequence analysis. The SeMet-*Tt*DERA protein was purified using the same method as that of native *Tt*DERA except for the addition of selenomethionine (LeMaster & Richards, 1985).

2.2. Functional analysis

The oligomerization state of the purified *Tt*DERA was examined by a dynamic light-scattering experiment using a DynaPro MS/X (Protein Solutions) instrument at a protein concentration of 20 mg ml^{-1} in 20 m*M* Tris–HCl pH 7.6 with 200 m*M* NaCl. Several measurements were recorded at 291 K and analyzed using the *DYNAMICS* software v.3.30 (Protein Solutions). A bimodal analysis resulted in a molecular weight of 84 kDa, which corresponds to four subunits and hence to the formation of homotetramers in solution.

The enzyme activity was assayed with 0.025–2 m*M* DRP in 0.1 *M* HEPES–NaOH buffer pH 7.4 in the presence of 0.3 m*M* NADH using a glyceraldehyde-3-phosphate dehydrogenase/triose-phosphate isomerase-coupled enzyme system (1 U ml^{-1}, Sigma G-1881) at 298 and 308 K by observing the decrease in NADH concentration as monitored at 340 nm. The DERA activity was determined following the procedure described for *Ec*DERA (Heine *et al.*, 2001). The Bradford method (Bradford, 1976) with bovine serum albumin as the standard was used for the determination of protein concentration.

2.3. Crystallization

The crystals used for structure determination were obtained by the microbatch method using NUNC HLA plates. The crystallization solution was prepared by mixing 1 µl 22 mg ml^{-1} *Tt*DERA and 1 µl precipitant solution containing 44% 2-methyl-2,4-pentanediol, 0.05 *M* magnesium chloride and 0.1 *M* Tris–HCl pH 7.9. Crystals grew to maximum dimensions of 0.2 × 0.2 × 0.3 mm after overnight incubation of the crystallization solution at 295 K. Selenomethionine (SeMet) substituted *Tt*DERA (LeMaster & Richards, 1985) was purified using a procedure similar to that of the native enzyme. SeMet-substituted *Tt*DERA crystals were obtained by mixing 1 µl protein solution at 20 mg ml^{-1}, 0.5 µl precipitant solution (1 *M* ammonium sulfate and 1 *M* sodium acetate) and 0.2 µl 30% 2-methyl-2,4-pentanediol pH 4.9. The initial crystallization conditions were established using the initial screen of 144 independent conditions implemented in the TERA automatic crystallization system (Sugahara & Miyano, 2002). Efforts to cocrystallize DRP substrate with the *Tt*DERA enzyme were not successful. However, it was possible to obtain DRP-bound *Tt*DERA crystals by soaking preformed crystals in a solution containing the ligand. A series of conditions varying the soaking time as well as the concentration of DRP substrate were examined. Finally, an 8 min

Table 1
Data-collection, phasing and refinement statistics.

Values in parentheses are for the highest resolution shell.

	Native	Complex	Remote	Peak	Edge
Wavelength (Å)	0.800	0.800	0.900	0.9793	0.9791
Space group	$P2_12_12_1$	$P2_12_12_1$	$P2_12_12_1$		
Unit-cell parameters (Å)	a = 64.280, b = 97.686, c = 137.918	a = 63.826, b = 96.907, c = 137.936	a = 64.028, b = 114.935, c = 119.406		
V_M (Å^3 Da^{-1})	2.3	2.3	2.4		
Content of the AU	Tetramer	Tetramer	Tetramer		
Resolution range (Å)	30.0–1.50 (1.55–1.50)	30.0–1.40 (1.45–1.40)	20.0–2.20 (2.28–2.20)	20.0–2.20 (2.28–2.20)	20.0–2.20 (2.28–2.20)
Reflections (measured/unique)	665297/137192	599735/165085	335453/45659	334940/45374	335517/45574
R_{merge} (%)†	6.7 (45.6)	4.8 (48.4)	8.3 (19.6)	7.7 (13.6)	6.9 (16.8)
Completeness (%)	98.5 (99.5)	98.0 (97.3)	99.9 (98.7)	100.0 (99.9)	100.0 (99.9)
Overall $\langle I/\sigma(I)\rangle$	12.6 (4.3)	15.3 (4.1)	13.4 (5.7)	15.6 (6.1)	13.7 (5.9)
Overall redundancy	4.85	3.63	7.34	7.38	7.36
Phasing (20.0–2.2 Å)					
R_{cullis} (centric/acentric)			0.52/0.60	0.60/0.65	
Phasing power (centric/acentric)			1.41/1.59	0.93/0.97	
Mean FOM after *RESOLVE* phasing (centric/acentric)					0.46/0.48
Refinement statistics					
Refinement resolution (Å)	30.0–1.50	30.0–1.40	20.0–2.20		
No. residues	845	843	843		
No. substrate atoms		52			
No. water molecules	481	442	398		
R_{cryst}/R_{free} (%)	19.6/21.3	20.1/21.0	21.0/23.0		
Ramachandran plot					
Residues in most favourable regions (%)	94.3	93.9	92.9		
Residues in additional allowed regions (%)	5.7	6.1	7.1		
R.m.s. deviations					
Bond lengths (Å)	0.004	0.004	0.006		
Bond angles (°)	1.29	1.28	1.30		

† $R_{merge} = \sum\sum_i |I(h) - I(h)_i| / \sum\sum_i I(h)$, where $I(h)$ is the mean intensity after rejections.

soak of the crystals in 100 m*M* substrate resulted in a map with clearly interpretable electron density for the ligand.

2.4. Data collection and structure determination

X-ray diffraction data sets were collected at 100 K using synchrotron radiation at beamlines BL45 (MAD data for the native) and BL26B1 (single-wavelength data for the complex), SPring-8, Japan using an R-AXIS V image-plate detector. The crystal-to-detector distance was set to 170 mm and images of 0.5° oscillation were collected for 25 s both for the native and the complex data sets. All data sets were processed using the program *HKL*2000 (Otwinowski & Minor, 1997). Native and ligand-complex crystals belong to the same space group, $P2_12_12_1$, with similar unit-cell parameters and consist of four molecules in the asymmetric unit. The calculated Matthews coefficient (Matthews, 1968) is 2.3 Å^3 Da^{-1}, which corresponds to a solvent-volume fraction of approximately 47%. For the SeMet crystal, an X-ray fluorescence spectrum was recorded and used to determine the wavelength optima for the MAD data collection [0.9793 Å (peak), 0.9791 Å (edge) and 0.9000 Å (remote)]. In order to record these data, the crystal-to-detector distance was set to 350 mm and images consisting of 1° oscillation were recorded for 60 s. Unit-cell parameters are different for the SeMet derivative when compared with those of the native and complex crystals, although they share the same space group.

The structure of SeMet-*Tt*DERA was initially determined at 2.2 Å resolution by the multiple anomalous dispersion (MAD) method (Hendrickson *et al.*, 1990). General handling of the scaled data was carried out with programs from the *CCP*4 suite (Collaborative Computational Project, Number 4, 1994). Ten Se-atom positions were determined using the program *SHELXS* (Sheldrick, 1990) and the phases were determined using *SOLVE* at 2.2 Å resolution (Terwilliger & Berendzen, 1999). Fourfold non-crystallographic symmetry (NCS) averaging was carried out based on the SeMet positions. Later, phases were improved by the density-modification program *DM* (Cowtan & Main, 1998). The resulting electron-density map was sufficient to build an initial model of the structure. The model for a monomer was built using the program *QUANTA* (Accelrys San Diego, CA, USA). The *Tt*DERA tetramer was constructed by applying NCS to the manually fitted subunit. The structure was then subjected to rigid-body refinement with NCS constraints using the *CNS* (Brünger *et al.*, 1998) program. For all the crystal forms, NCS restraints were imposed on the initial models, but as the refinement proceeded the restraints were relaxed and finally removed. Each cycle of refinement with bulk-solvent and overall anisotropic *B*-factor corrections consisted of rigid-body refinement, simulated annealing incorporating the slow-

cool protocol, positional refinement and *B*-factor refinement (individual or group). Several cycles of model building and refinement yielded the final model. The structure of the native crystal was determined by the molecular-replacement program *AMoRe* (Navaza, 1994) using the SeMet *Tt*DERA tetramer as the search model. Native and DRP-liganded structures were refined at 1.5 and 1.4 Å resolution, respectively. The electron densities of all residues were well defined and continuous in the electron-density maps of SeMet, native and DRP-liganded structures. Structural evaluations of the final models were performed using *PROCHECK* (Laskowski *et al.*, 1993). Molecular-surface areas were calculated using *QUANTA*. Figures were prepared using *ESPript* (Gouet *et al.*, 2003) for Fig. 2, and *MOLSCRIPT* (Kraulis, 1991), *BOBSCRIPT* (Esnouf, 1999) and *RASTER3D* (Merritt & Bacon, 1997) for Figs. 1, 3, 4(*b*) and 5. Details of data collection, phasing and refinement are summarized in Table 1.

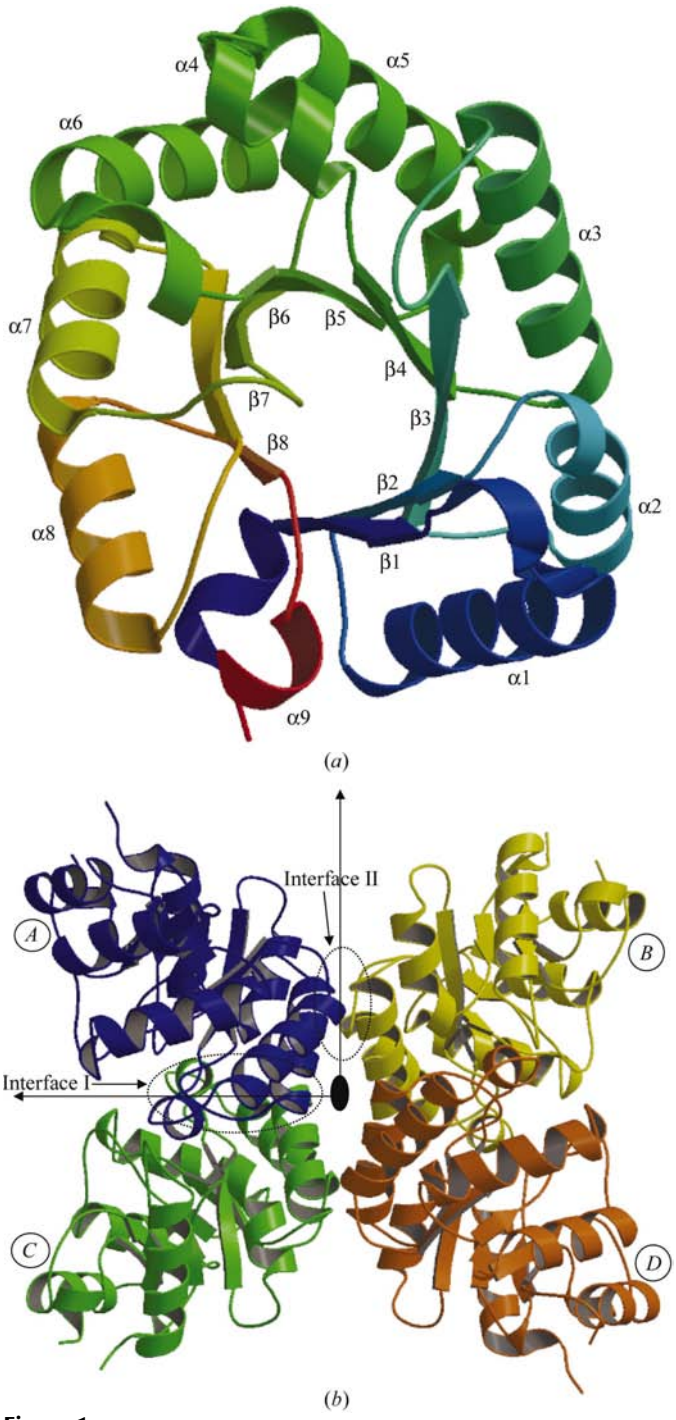

Figure 1
Ribbon representation of *T. thermophilus* DERA. (*a*) Protomer structure of *Tt*DERA. Secondary structures are labelled. The N- and C-termini are coloured blue and red, respectively. (*b*) Tetramer structure of *Tt*DERA. Subunits *A*, *B*, *C* and *D* are coloured blue, yellow, green and orange, respectively. Molecular local 222 symmetry is depicted by crystallographic symbols.

Table 2
R.m.s. deviations with *Tt*DERA (PDB code 1j2w).

The coordinates compared are from *Ap*DERA (1n7k), *Ec*DERA (1jcl), KDPG aldolase from *E. coli* (1eua), transaldolase B from *E. coli* (1ucw), aldolase from human muscle (4ald), aldolase from rabbit muscle (FBP aldolase; 1ado) and glucosamine 6-phosphate deaminase from *E. coli* (1fqo).

Enzyme	R.m.s.d. (Å)	Residues fitted	Sequence identity (%)	Secondary-structure identity (%)
1n7k	1.38	207	37.7	89.1
1jcl	1.58	212	32.1	89.0
1eua	2.26	156	14.2	79.0
1ucw	2.74	160	14.3	72.3
4ald	3.32	180	9.2	67.2
1ado	3.36	180	9.1	72.0
1fqo	3.94	86	6.2	33.5

3. Results and discussion

3.1. Structure determination and model quality

The final native model comprises 6338 protein atoms from four independent molecules in the asymmetric unit of the crystal, together with 481 water molecules. Of the four *Tt*DERA protomers, the *A*, *B* and *C* molecules comprise residues 1–212 and the *D* molecule comprises residues 1–211; C-terminal residues with no density are assumed to be disordered. The protein molecules in the native and DRP-liganded forms have acceptable stereochemical parameters. The program *PROCHECK* (Laskowski *et al.*, 1993) indicates that 94% of the non-glycine residues are in the most favoured region of the Ramachandran map and no residues are present in the disallowed region.

3.2. Overall structure

The crystal structures of *Tt*DERA in the native, SeMet-substituted and DRP-liganded forms have been determined. In all forms, the *Tt*DERA protomer has an identical classical $(\alpha/\beta)_8$ TIM-barrel fold (Fig. 1*a*) as in other class I aldolases including *E. coli* (*Ec*DERA) and *A. pernix* (*Ap*DERA) enzymes. The asymmetric unit of each crystal form consists of four monomers consistent with a homotetramer of molecular symmetry 222 (Fig. 1*b*). The tetrameric state of *Tt*DERA observed in the crystal is consistent with the results of dynamic light-scattering experiments, which show that the enzyme is also present as a tetramer in solution (see §2). Each subunit of the tetramer interacts with two neighbouring subunits. We

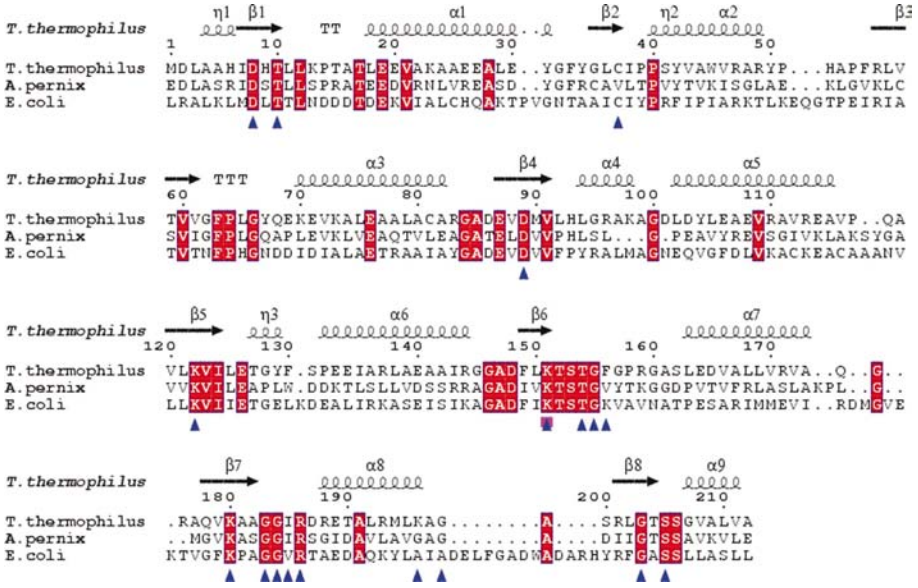

Figure 2
Structure-based sequence alignment of DERAs from *T. thermophilus*, *A. pernix* and *E. coli* and secondary-structure assignment of the *T. thermophilus* enzyme. Invariant residues are coloured red. Residues involved in the substrate binding and the reactive lysine residue are indicated by blue triangles and a pink box, respectively.

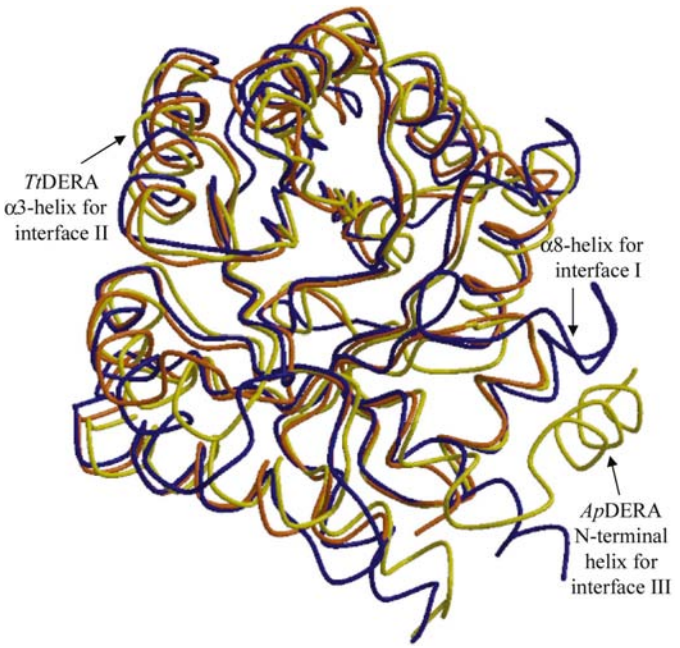

Figure 3
Structural alignment of *Tt*DERA (orange), *Ec*DERA (blue) and *Ap*DERA (yellow).

define the interface between the subunits *A* and *C* as interface I and that between the subunits *A* and *B* as interface II (Fig. 1*b*). In *Tt*DERA, each interface is composed of several polar and non-polar interactions, a plausible reflection of the biological importance of the tetramer. The intersubunit arrangements of the SeMet and native tetramers are very similar. The r.m.s. deviation of the corresponding C^{α} positions is less than 0.4 Å. Thus, the observed large unit-cell differences between SeMet and other crystal forms (Table 1) mainly arise from differences in molecular packing resulting from different crystallization conditions. In the DRP-liganded form, electron density corresponding to a carbinolamine was observed, probably owing to the reaction of the aldehyde of 2-deoxyribose-5-phosphate and the active-site Lys151. The substrate is bound in the central pocket of the TIM barrel, covalently anchored to Lys151 on strand β6 and stabilized by polar interactions.

3.3. Residue conservation

The r.m.s. deviations of the corresponding C^{α} atoms when the native structure of *Tt*DERA was aligned using the program *LSQKAB* (Kabsch, 1976) with the structures of class I aldolases available in the PDB are listed in Table 2. Also listed are the percentages of sequence and secondary-structure identity between these aldolases and *Tt*DERA. The secondary-structure elements were determined using the program *DSSP* (Kabsch & Sander, 1983). The length of the helix α8 is shortened in *Tt*DERA and *Ap*DERA compared with *Ec*DERA. Alignments of the sequences and structures of *Ec*DERA and *Ap*DERA with *Tt*DERA are shown in Figs. 2 and 3, respectively. Schiff-base formation between the carbonyl of the substrate and an invariant lysine residue is the most important characteristic of class I aldolases (Gefflaut *et al.*, 1995). In order to figure out the required common structural feature for the catalysis, we focused on the structural conservation of the reactive lysine residues. The reactive lysines of all class I aldolases are located on the same strand and in the same position, except in transaldolase. In *Ec*DERA and *Ap*DERA, reactive Lys167 on the strand β6 forms the Schiff base. In FBP aldolase (Blom & Sygusch, 1997) the Schiff base is formed at Lys229, also on strand β6. In transaldolase B only (Jia *et al.*, 1997), Lys132, which forms the Schiff base, occurs on strand β4. In *E. coli* KDPG aldolase (Allard *et al.*, 2001), Lys133, which forms the Schiff base, is on strand β6 and Glu45 is considered to act as a general base. These observations suggest a similar configuration for the catalytic residue on strand β6 that forms the covalent intermediate Schiff base in the class I aldolases.

A multiple sequence alignment of DERA orthologues (Fig. 2) was obtained in order to identify the functionally important residues in DERA. Mapping of the conserved residues on the molecular surface clearly revealed a conservation pattern. Most of the surface-invariant residues correspond to those proposed to be directly involved in substrate binding or catalysis, *viz*. Asp8, Thr10, Asp89, Lys122, Lys151, Thr154, Gly155, Lys180, Gly183, Gly184, Arg186, Gly203 and Ser205.

All 18 organisms examined (not shown) share this conservation pattern, confirming the functional importance of these residues. On the other hand, residues involved in the polar interaction between the subunits are not well conserved. These residues contribute to the oligomeric state of DERA and hence the residue conservation is not necessarily required for the potential role of the oligomeric state.

Table 3
Comparison of surface areas.

	Accessible surface area (Å^2)	Interface contact area (Å^2)	Residue No.
E. coli DERA			
Dimer (interface I)	19489	585	
Monomer	10214		260
T. thermophilus DERA			
Tetramer	28436	4230	
AB dimer (interface II)	17346	489	
AC dimer (interface I)	15305	1519	
Monomer	9162		220
A. pernix DERA			
Tetramer	31962	4802	
AB dimer (interface III)	18478	1052	
AC dimer (interface I)	17884	1349	
Monomer	10292		234

3.4. Reaction mechanism

We measured the enzymatic activity of *Tt*DERA at 298 and 308 K. The k_{cat} (s^{-1}) and K_m (μM) are 5.0 and 75 at 298 K and 11.4 and 56 at 308 K, respectively. The reported parameters for *Ec*DERA are 68 and 640, respectively, at 298 K (Heine *et al.*, 2001). The extrapolated (assuming a twofold increase in activity for every 10 K rise in the temperature) activity of *Tt*DERA at the higher living temperature of *T. thermophilus* of about 348 K is comparable to that of *Ec*DERA at room temperature. A schematic diagram of the enzyme–substrate topology is shown in Fig. 4(*a*). We refined the crystal structure of the ligand without applying any geometrical restraints. The high-resolution data at 1.4 Å was helpful in identifying the covalent bond geometry between Lys151 and the ligand DRP (Figs. 4*b* and 4*c*). The bond distance between Lys151 N^{ζ} and the first C atom (C1) of DRP is 1.38 Å, which is very similar to that observed in *Ec*DERA. The substrate with phosphate moiety has an extended conformation, which is similar to the *Ec*DERA but different from FBP aldolase, where the substrate exists in cyclic form. The carbinolamine, a covalent intermediate in *Tt*DERA, is presumably a product of the reaction between the aldehyde substrate and Lys151. This reaction occurs by a mechanism probably similar to that proposed for *Ec*DERA (Heine *et al.*, 2001). The networks of salt bridges, Lys151–Asp89 and Lys180–Asp8–Arg201, have been reported to be important for making the uncharged Lys151 act as a nucleophile, attacking the substrate carbonyl C atom (Fig. 4*a*). The carbonyl O atom of the substrate may be stabilized by the active-site water molecule, Wat40. This water molecule has been observed in all reported DERA structures and is strictly conserved. We compared the crystallographically determined bond lengths and angles of the covalent intermediates with theoretically expected values. In *Tt*DERA and *Ec*DERA carbinolamine complexes, the observed angles are similar and agree well with the theoretical values. The arrangement around the first C atom of the substrate is tetrahedral: the N^{ζ}—C1 bond is 1.38 Å, the N^{ζ}—C1—C2 angle is 117.1°, the O1—C1—C2

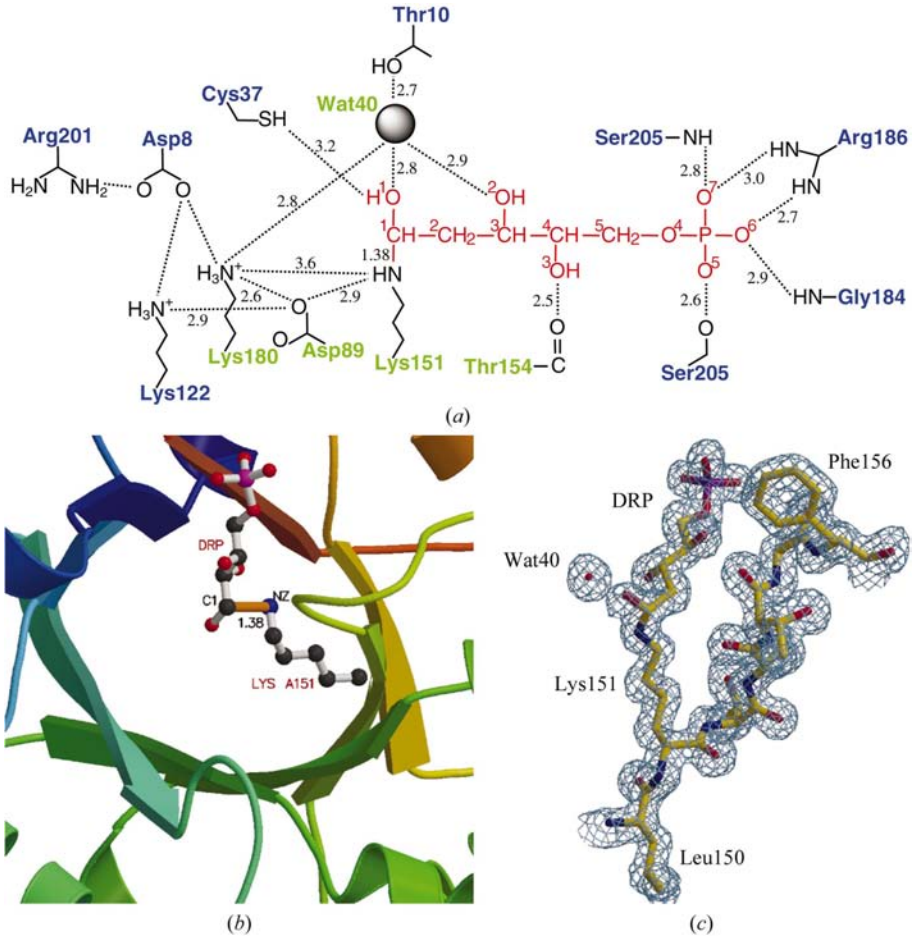

Figure 4
(*a*) Topology diagram of *T. thermophilus* DERA–substrate (DRP) interactions. The residues and water molecules involved in the catalysis are coloured green. The substrate is shown in red. Hydrogen bonds are indicated by dotted lines and lengths are given in Å. (*b*) The substrate covalently bound to the pocket of the TIM-barrel strand β6. The substrate and Lys151 residue are depicted in ball-and-stick representation. (*c*) The electron density in the vicinity of the DERA active site with the carbinolamine-bound model. The $2F_o - F_c$ electron density contoured at 2σ is shown in blue.

angle is 113.0° and the N^{ζ}—C1—O1 angle is 108.5°. Compared with these, the values found in the KDPG aldolase pyruvate carbinolamine complex are very different: the N^{ζ}—C1 bond is 1.48 Å, the N^{ζ}—C1—C2 angle is 79.4°, the O1—C1—C2 angle is 109.0°and the N^{ζ}—C1—O1 angle is 140.3°. These results suggest that the reaction mechanism of *Tt*DERA is similar to that of *Ec*DERA.

Table 4
The contribution of intersubunit interactions to the thermal stability of DERAs.

Values were calculated per subunit. Accessible surface-area (ASA) values in Å^2 were calculated using the Connolly surface (Connolly, 1993). ΔG and $\Delta\Delta G$ values are in kJ mol^{-1}.

	Hydrophobic interaction				Hydrogen bond			
Protein	Δ(ASA) (C/S)	Δ(ASA) (N/O)	ΔG	$\Delta\Delta G$	No.	ΔG	$\Delta\Delta G$	Ion pair
*Ec*DERA	402	247	68	0	1	9	0	0
*Tt*DERA	1479	635	255	187	5.5	47	38	0.75
*Ap*DERA	1795	676	311	243	6.5	55	46	0

3.5. Biological implication of the oligomeric state

The biological role of the oligomeric state of DERA is not understood. It has been experimentally demonstrated that the *Ec*DERA monomer possesses all the necessary components for catalysis and that it is dimeric in solution (Heine *et al.*, 2001). Recently, the crystal structure of *Ap*DERA from a hyperthermophilic archeon has been reported (Sakuraba *et al.*, 2003). As in *T. thermophilus*, in this archeon the enzyme also exists as a tetramer in solution.

In order to evaluate the importance of oligomeric interfaces in DERA, structural superposition of *Tt*DERA, *Ap*DERA and *Ec*DERA oligomers was performed. The dimer interface I consisting of the α8 helix is similar in *Tt*DERA and *Ap*DERA but substantially different in *Ec*DERA (Figs. 3 and 5*a*). The tetramer interface of *Tt*DERA is very different from that of *Ap*DERA. We designated another tetramer interface of *Ap*DERA as interface III (Figs. 3 and 5*b*). The tetramer interface involves the α3 helix in *Tt*DERA (interface II) and the N-terminal α-helix in *Ap*DERA (interface III). It was thought that the formation of the tetramer arises from the presence of the N-terminal helix in *Ap*DERA (Sakuraba *et al.*, 2003). The present structure of *Tt*DERA clearly demonstrates that the N-terminal helix is not essential for the formation of the tetramer. The observed tetrameric oligomerization state in both the thermophiles suggests that the biological role of the oligomeric state of DERA is to enhance the thermal stability of the enzyme. It does not appear to be important for the catalytic function itself.

A comparison of the molecular-surface areas of *Tt*DERA, *Ec*DERA and *Ap*DERA is made in Table 3. The buried surface area of the interface I in *Tt*DERA is larger than those of the other two enzymes. However, the tetramer interface of *Tt*DERA (interface II) is smaller than that of *Ap*DERA (interface III). In *Tt*DERA, the small discrepancy observed

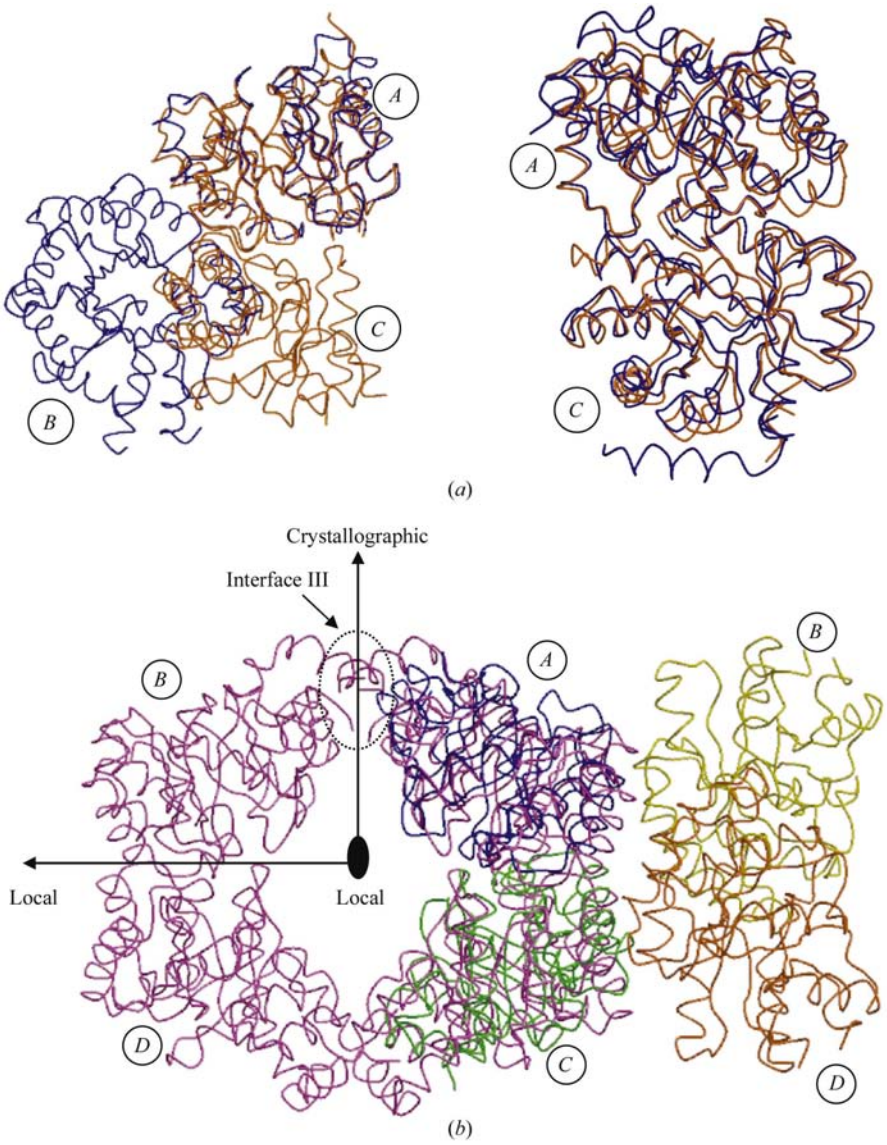

Figure 5
(*a*) Superposition of *Tt*DERA *AC* dimer (orange) with the corresponding dimers of *Ec*DERA (left) and *Ap*DERA (right). The respective *A* subunits were used for superposition. (*b*) Structural alignment of *Tt*DERA and *Ap*DERA (pink) tetramers at the *AC* dimers. The colouring and perspective of *Tt*DERA are similar to those in Fig. 1(*b*). The molecular 222 symmetry of *Ap*DERA is depicted by crystallographic symbols.

between the total tetramer contact area and twice the sum of the areas of interfaces I and II indicates the presence of an additional minor interface of about 100 Å^2 between *A* and *D* or *B* and *C* subunits. We also calculated the buried surface area for the polar and non-polar atoms separately (Funahashi *et al.*, 2001) and found that both hydrophilic and hydrophobic interactions are significant at both the dimer and tetramer interfaces. These comparisons revealed that DERA is more stable in the tetrameric form when compared with the dimeric form. A larger contact area in the thermostable enzymes *Tt*DERA and *Ap*DERA therefore indicates that the tetrameric structure is required for higher thermal stability. To estimate the energy of intersubunit interaction quantitatively, we calculated the estimated value of dissociation ΔG for hydrophobic interaction based on the accessible surface area (ASA) of the non-polar and polar atoms (Tanaka *et al.*, 2001) and for hydrogen bonding, assuming 8.5 kJ mol^{-1} for a 3 Å bond (Takano *et al.*, 1999) among the three DERAs (Table 4). The intersubunit interactions of *Tt*DERA and *Ap*DERA have larger ΔG values for both hydrophobic interactions and hydrogen bonding compared with *Ec*DERA. A remarkable increase in the number of ion pairs in thermophilic organisms was not observed. These results suggest that the hydrophobic interaction and hydrogen bonding at the oligomeric interface would contribute to the thermal stability of this enzyme.

In conclusion, the monomeric structures of DERAs in these three organisms are very similar. However, the oligomeric arrangements are different. We suggest that the oligomeric state of DERA contributes to the thermal stability of this protein family. Triosephosphate isomerase, another $(\alpha/\beta)_8$-barrel enzyme, is a dimer in most organisms, with the exception of two thermophiles *T. maritima* and *Pyrococcus woesi*, where it occurs as a tetramer in solution (Walden *et al.*, 2001). Oligomerization might be one of the fundamental strategies for the structural stabilization of enzymes in thermophilic organisms.

NKL solved the structure and wrote the paper, IS contributed to the early stages of the structural analysis, NO performed the enzymatic experiment, YN contributed the large-scale protein production, MS contributed the automated crystallization, SK and SY provided the plasmid of *Tt*DERA, MM organized the research and NK supervised the work. The authors would like to thank the technical staff of the High-throughput Factory, Y. Ukita for protein production and Y. Nakamura and M. Sawano for crystallization. We also thank K. Yutani for useful discussions, M. R. N. Murthy for critical reading of the manuscript and the beamline staff for assistance during data collection at beamlines BL26B1 and BL45 of SPring-8. This work (TT0501/HTPF00315) was supported by 'National Project of Protein Structural and Functional Analysis' funded by the MEXT of Japan.

References

Allard, J., Grochulski, J. & Sygusch, J. (2001). *Proc. Natl Acad. Sci. USA*, **98**, 3679–3684.
Barbas, C. F., Wang, Y. F. & Wong, C.-H. (1990). *J. Am. Chem. Soc.* **112**, 2013–2014.
Blom, N. & Sygusch, J. (1997). *Nature Struct. Biol.* **4**, 36–39.
Bradford, M. M. (1976). *Anal. Biochem.* **72**, 248–254.
Brünger, A. T., Adams, P. D., Clore, G. M., DeLano, W. L., Gros, P., Grosse-Kunstleve, R. W., Jiang, J.-S., Kuszewski, J., Nilges, M., Pannu, N. S., Read, R. J., Rice, L. M., Simonson, T. & Warren, G. L. (1998). *Acta Cryst.* D**54**, 905–921.
Collaborative Computational Project, Number 4 (1994). *Acta Cryst.* D**50**, 760–763.
Connolly, M. L. (1993). *J. Mol. Graph.* **11**, 139–141.
Cowtan, K. & Main, P. (1998). *Acta Cryst.* D**54**, 487–493.
Esnouf, R. M. (1999). *Acta Cryst.* D**55**, 938–940.
Funahashi, J., Takano, K. & Yutani, K. (2001). *Protein Eng.* **14**, 127–134.
Gefflaut, T., Blonski, C., Perie, J. & Willson, M. (1995). *Prog. Biophys. Mol. Biol.* **63**, 301–340.
Gijsen, H. J. M., Qiao, L., Fitz, W. & Wong, C.-H. (1996). *Chem. Rev.* **96**, 443–474.
Gouet, P., Robert, X. & Courcelle, E. (2003). *Nucleic Acids Res.* **31**, 3320–3323.
Heine, A., DeSantis, G., Luz, J. G., Mitchell, M., Wong, C.-H. & Wilson, I. A. (2001). *Science*, **294**, 369–374.
Hendrickson, W. A., Horton, J. R. & LeMaster, D. M. (1990). *EMBO J.* **9**, 1665–1672.
Jia, J., Schorken, U., Lindqvist, Y., Sprenger, G. A. & Schneider, G. (1997). *Protein Sci.* **6**, 119–124.
Kabsch, W. (1976). *Acta Cryst.* A**32**, 922–923.
Kabsch, W. & Sander, C. (1983). *Biopolymers*, **22**, 2577–2637.
Kajimoto, T., Liu, K. K.-C., Chen, L. & Wong, C.-H. (1991). *J. Am. Chem. Soc.* **113**, 6678–6680.
Koeller, K. M. & Wong, C.-H. (2001). *Nature (London)*, **409**, 232–240.
Kraulis, P. J. (1991). *J. Appl. Cryst.* **24**, 946–950.
Laemmli, U. K. (1970). *Nature (London)*, **227**, 680–685.
Laskowski, R. A., Macarthur, M. W., Moss, D. S. & Thornton, J. M. (1993). *J. Appl. Cryst.* **26**, 283–291.
LeMaster, D. M. & Richards, F. M. (1985). *Biochemistry*, **24**, 7263–7268.
Machajewski, T. D. & Wong, C.-H. (2000). *Angew. Chem. Int. Ed. Engl.* **39**, 1352–374.
Matthews, B. W. (1968). *J. Mol. Biol.* **33**, 491–497.
Merritt, E. A. & Bacon, D. J. (1997). *Methods Enzymol.* **277**, 505–524.
Navaza, J. (1994). *Acta Cryst.* A**50**, 157–163.
Otwinowski, Z. & Minor, W. (1997). *Methods Enzymol.* **276**, 307–326.
Sakuraba, H., Tsuge, H., Shimoya, I., Kawakami, R., Goda, S., Kawarabayasi, Y., Katunuma, N., Ago, H., Miyano, M. & Ohshima, T. (2003). *J. Biol. Chem.* **278**, 10799–10806.
Sheldrick, G. M. (1990). *Acta Cryst.* A**46**, 467–473.
Sugahara, M. & Miyano, M. (2002). *Tanpakushitsu Kakusan Koso*, **47**, 1026–1032.
Takano, K., Yamagata, Y., Funahashi, J., Hiroki, Y., Kuramitsu, S. & Yutani, K. (1999). *Biochemistry*, **38**, 12698–12708.
Tanaka, H., Chinami, M., Mizushima, T., Ogasawara, K., Ota, M., Tsukihara, T. & Yutani, K. (2001). *J. Biochem.* **130**, 107–118.
Terwilliger, T. C. & Berendzen, J. (1999). *Acta Cryst.* D**55**, 849–861.
Valentin-Hansen, P., Boetius, F., Hammer-Jespersen, K. & Svendsen, I. (1982). *Eur. J. Biochem.* **125**, 561–566.
Walden, H., Bell, S. G., Russell, R. J. M., Siebers, B., Hensel, R. & Taylor, G. L. (2001). *J. Mol. Biol.* **306**, 745–757.